

CountCluster: Training-Free Object Quantity Guidance with Cross-Attention Map Clustering for Text-to-Image Generation

Joohyeon Lee, Jin-Seop Lee, Jee-Hyong Lee*

Sungkyunkwan University, Suwon, South Korea
{leeju001, wlstjq0602, john}@skku.edu

Abstract

Diffusion-based text-to-image generation models have demonstrated strong performance in terms of image quality and diversity. However, they still struggle to generate images that accurately reflect the number of objects specified in the input prompt. Several approaches have been proposed that rely on either external counting modules for iterative refinement or quantity representations derived from learned tokens or latent features. However, they still have limitations in accurately reflecting the specified number of objects and overlook an important structural characteristic—The number of object instances in the generated image is largely determined in the early timesteps of the denoising process. To correctly reflect the object quantity for image generation, the highly activated regions in the object cross-attention map at the early timesteps should match the input object quantity, while each region should be clearly separated. To address this issue, we propose *CountCluster*, a method that guides the object cross-attention map to be clustered according to the specified object count in the input, without relying on any external tools or additional training. The proposed method partitions the object cross-attention map into k clusters at inference time based on attention scores, defines an ideal distribution in which each cluster is spatially well-separated, and optimizes the latent to align with this target distribution. Our method achieves an average improvement of 18.5%^p in object count accuracy compared to existing methods, and demonstrates superior quantity control performance across a variety of prompts. Code will be released at: <https://github.com/JoohyeonL22/CountCluster>.

Introduction

Generative models have led to remarkable progress in the field of text-to-image generation, where visual content is synthesized solely from natural language descriptions. While early approaches were based on GANs (Goodfellow et al. 2014; Radford, Metz, and Chintala 2016; Karras, Laine, and Aila 2019), diffusion models (Ho, Jain, and Abbeel 2020; Dhariwal and Nichol 2021; Rombach et al. 2022) have recently demonstrated superior performance in terms of image quality and diversity. With the development of diffusion models, various applications including image synthesis (Gu et al. 2022; Saharia et al. 2022; Ramesh et al.

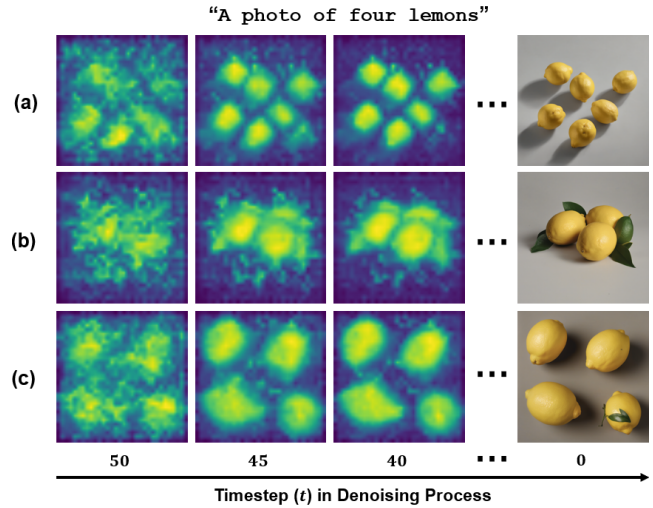


Figure 1: Generated images using SDXL (Podell et al. 2024) for the prompt “A photo of four lemons”. The left side shows the cross-attention maps of “lemons” at timesteps $t = 50, 45, 40$ during the denoising process, while the right side shows the final generated image at timestep $t = 0$. (a), (b), and (c) are results under the same conditions with different seeds. Among them, (a) and (b) are failure cases with incorrect instance counts, while (c) is a successful case with the correct number of instances. It can be observed that the positions and number of instances are mostly determined at the early timesteps of the denoising process.

2021), inpainting (Meng et al. 2022; Lugmayr et al. 2022; Nichol et al. 2022; Couairon et al. 2023), and visual editing (Kawar et al. 2023; Tumanyan et al. 2023; Cao et al. 2023) have been increasingly adopted in practical scenarios. This trend highlights a growing need to generate images that faithfully reflect the user’s intent, including the specified number of instances. However, diffusion models still struggle to generate images that correctly reflect the exact number of instances of each object described in the input text (e.g., “a photo of four lemons”) (Paiss et al. 2023; Hu et al. 2023; Wen et al. 2023).

Recently, several studies have been conducted to address the limitations of reflecting object quantity in gener-

*Corresponding author

ated images. Existing approaches can be categorized into two types: iterative refinement-based methods and Quantity-representation guided methods. Iterative refinement-based approaches (Binyamin et al. 2024; Kang et al. 2025) estimate the number of object instances during the image generation process and either regenerate the image or iteratively refine it and re-estimate the count. Quantity-representation guided approaches (Zafar, Wolf, and Schwartz 2024; Zhang, Chen, and Lee 2023) encode quantity information by either defining new tokens to learn quantity representations or extracting latent vectors that control the number of instances. Then, they utilize the quantity representation to guide the generation of other object categories with the same count. These approaches show improvements over a naive Stable Diffusion (Rombach et al. 2022; Podell et al. 2024), however, they still struggle to generate images with the exact number of objects. Importantly, they overlook the most essential factor for quantity control—the number of instances in the generated image is mostly determined during the early timesteps of the diffusion process.

For diffusion models, highly activated regions in the object cross-attention map, which indicate strong attention to the corresponding object token, are strongly correlated with the object locations in the generated image (Hertz et al. 2023). As shown in the cross-attention maps for “lemons” token in fig. 1, the positions and number of objects are largely determined at the early timesteps of the generation process. When the number of clusters of highly activated regions in the object cross-attention map at early timesteps exceeds the object quantity specified in the input prompt, the generated image tends to contain more objects, as shown in fig. 1(a). In contrast, when the boundaries between activated regions are ambiguous and overlapping, some objects may be merged during the generation process, resulting fewer object instances being generated, as shown in fig. 1(b). Therefore, to ensure that the number of objects in the generated image reflects the quantity specified in the text prompt, the number of clusters of highly activated regions in the object cross-attention map at the early timesteps should exactly match the intended object count, and each region should also be sufficiently distinguished, as shown in fig. 1(c).

In addition, existing methods (Binyamin et al. 2024; Kang et al. 2025; Zafar, Wolf, and Schwartz 2024; Zhang, Chen, and Lee 2023) rely on external tools such as object counting and layout generation, or require training quantity-representations to encode instance count information. As a result, they incur substantial computational costs and time overhead, making practical deployment of quantity control techniques challenging. Therefore, it is necessary to reflect quantity information without requiring additional modules and training.

In this paper, we propose *CountCluster*, a method that generates object instances in the correct number while minimizing inference cost and time, without relying on any external tools or additional training. The proposed method guides the denoising process by clustering object cross-attention maps to reflect the intended instance count.

To achieve this, our method aims to ensure that the highly activated regions in the object cross-attention map during the

denoising process are sufficiently separated and match the number of instances specified in the input prompt. To this end, we form k clusters based on the attention scores in the object cross-attention map and define a target distribution that encourages these clusters to be spatially well-separated. We then design a loss function that guides the distribution of each cluster to align with the target distribution and apply training-free latent optimization during inference based on this objective. As a result, the highly activated regions in the cross-attention map become clearly separated according to the specified quantity, leading to the generation of images with the correct number of object instances.

The proposed method achieves an average improvement of 18.5%p in instance count accuracy compared to existing approaches. It also demonstrates the ability to generate visual scenes with correct quantity control across diverse prompts. Importantly, it operates solely by guiding the object cross-attention map during denoising process without requiring any additional training or external modules, resulting in higher efficiency and easier applicability than prior methods.

Related Work

Image Generation with Accurate Object Count

Despite recent advances, text-to-image models often fail to accurately reflect the number of objects explicitly specified in prompts (Paiss et al. 2023; Hu et al. 2023). To address this limitation, various approaches have been proposed. To address this limitation, various approaches have been proposed to improve the accuracy of object quantity in generated images. Among them, iterative refinement methods (Binyamin et al. 2024; Kang et al. 2025) estimate the number of object instances during the image generation process and iteratively refine or regenerate the image based on the estimated count.

Another line of research defines count tokens to explicitly train models for quantity control (Zafar, Wolf, and Schwartz 2024), or leverages quantity-representation guided approaches (Zhang, Chen, and Lee 2023), which extract numerical representation vectors encoding numerical information from the CLIP (Radford et al. 2021) embedding space.

While both approaches enhance object quantity control, they fail to resolve a fundamental structural limitation: the number of activated regions in the cross-attention maps during image generation often misaligns with the intended object count. Consequently, despite improvements in quantity control, the generated images frequently fail to faithfully represent the specified number of objects.

Latent Optimization via Attention Guidance

Training-free latent optimization have been actively explored to precisely control the output of pretrained text-to-image generation models. In particular, various approaches leveraging cross-attention maps have been proposed.

Image generation methods that leverage cross-attention maps are based on the observation that regions with high attention scores for a given text token tend to reflect the corresponding concept more strongly in the generated image

(Hertz et al. 2023). Building on this insight, Attend-and-Excite (Chefer et al. 2023) addresses the problem of subject neglect—where objects mentioned in the text prompt fail to appear in the image. To this end, it introduces a loss function based on normalized cross-attention scores, which is used to iteratively optimize the latent representation. Subsequently, a number of studies (Agarwal et al. 2023; Rassin et al. 2023; Meral et al. 2024; Guo et al. 2024; Weimin, Jieke, and Meng 2025) have proposed similar latent optimization strategies, primarily aiming to mitigate subject neglect by either reinforcing attention to specific tokens.

Such methods have the advantage of enabling the regulation of object presence without modifying the pretrained diffusion model. However, they primarily focus on binary presence or absence, and therefore face structural limitations when it comes to precisely controlling quantitative attributes such as object count.

Proposed Method

In diffusion models, the cross-attention map corresponding to an object token plays a critical role in determining the number and location of objects in the generated image. When the object cross-attention map fails to form sufficiently distinguished activation regions, or the number of highly activated regions does not match the number of objects (k) specified in the input prompt, the generated image tends to exhibit object count errors.

To address these issues, we propose *CountCluster*, a training-free method that ensures that the clustering of highly activated regions in the object cross-attention map matches the number of objects specified in the input, while encouraging clearly separated activation regions. The proposed method consists of the following three steps: (1) partition the cross-attention map into k clusters, (2) define an ideal target distribution in which each cluster corresponds to a distinct activation region, and (3) perform latent optimization to align the cluster distribution with the defined target.

Initializing Cross-Attention Cluster

To generate an image that contains the number of object instances specified in the input text, it is essential to obtain k well-separated activation regions in the object cross-attention map. To this end, we normalize the object cross-attention map and partition it into k clusters based on the attention scores.

First, only patches with attention scores greater than or equal to a predefined threshold τ are considered for clustering, while those below τ are excluded. As illustrated in the cross-attention map visualization in fig. 1, only patches with sufficiently high attention scores in the normalized cross-attention map are directly associated with the generation of actual objects in the image. This procedure prevents irrelevant background regions or noise from being included in the clusters and ensures that clustering is focused solely on the meaningful activation regions that contribute to object generation.

Subsequently, the top- k patches with the highest attention scores are selected as cluster centers. To ensure that each

Algorithm 1: Cluster Center Selection from Object Cross-Attention Map

Input: Cross-attention map of object token A_c , number of object instances k , minimum distance d

Output: Cluster centers $\mathcal{C} = \{c_1, \dots, c_k\}$

```

1: Initialize  $\mathcal{C} \leftarrow \{\}$ 
2:  $\mathcal{S} \leftarrow \text{argsort}_{(x,y)} A_c(x, y)$  in descending order
3: for each  $(x, y) \in \mathcal{S}$  do
4:   if  $\forall c \in \mathcal{C}, \|(x, y) - c\|_2 \geq d$  then
5:     Add  $(x, y)$  to  $\mathcal{C}$ 
6:   end if
7:   if  $|\mathcal{C}| = k$  then
8:     break
9:   end if
10: end for
11: return  $\mathcal{C}$ 

```

cluster represents a distinct object without merging with others, a minimum distance is enforced between the selected cluster centers. Thus, we define the following minimum distance constraint d :

$$\|c_i - c_j\|_2 \geq d = \frac{H}{k} \quad \text{for all } i \neq j \quad (1)$$

Here, c_i and c_j denote the positions of two distinct cluster centers, and H refers to the height (or width) of the attention map. Since this study generating square-shaped images, we assume a cross-attention map A_c where $H = W$. Algorithm 1 illustrates the procedure for selecting cluster centers under these conditions. Once the cluster centers are determined, each patch in the cross-attention map is assigned to its nearest center.

Constructing Target Distributions for Clusters

After forming clusters around k activation regions within the normalized cross-attention map, we define a target distribution to encourage each cluster to correspond to a distinct and well-separated activation region.

Simply dividing regions based on attention scores may result in the presence of multiple sub-clusters within a single cluster, which can lead to the generation of multiple objects from a single cluster. To ensure that each cluster generates only one object, there must be only one dominant density region within each cluster. Accordingly, we define a target distribution in which the attention score gradually decreases from the cluster center toward the boundary, and encourage the actual cross-attention distribution to follow this form.

We use a 2D Gaussian function as the target distribution. The Gaussian function is defined to have a value of 1 at the cluster center and to decay to the threshold value τ , used during clustering, at the cluster boundary. This encourages all patches within a cluster to maintain an attention score above τ , which is the minimum level required to contribute to object generation. This design aims to ensure that each cluster focuses on a single object while avoiding significant distortion of the original cross-attention map distribution. To construct this Gaussian distribution, we determine σ based on the distance r between the cluster center and the cluster

boundary as follows:

$$\sigma = \sqrt{\frac{r^2}{-2\log(\tau)}} \quad (2)$$

From this, the target distribution for each cluster is defined as follows:

$$P(\mathbf{x}) = \exp\left(-\frac{\|\mathbf{x} - \boldsymbol{\mu}\|^2}{2\sigma^2}\right) \quad (3)$$

Here, \mathbf{x} denotes the coordinates of each patch in the attention map, and $\boldsymbol{\mu}$ represents the position of the cluster center.

Latent Optimization via Clustering Loss

Once each cluster and its corresponding target distribution are defined within the cross-attention map, we design a loss function to encourage the distribution of each cluster to resemble its target distribution. The similarity between the attention distribution $Q(x)$ of each cluster within the cross-attention map and its corresponding target distribution $P(x)$ is measured using the KL divergence (Kullback and Leibler 1951).

As the number of clusters increases, the total KL loss increases, while the image area occupied by each individual cluster decreases, which tends to reduce the KL loss of each cluster. To account for this effect and keep the total KL loss at a comparable scale regardless of the number of clusters, we normalize the total loss by \sqrt{k} and define the overall loss as follows:

$$\begin{aligned} L_{\text{KL}} &= \frac{1}{\sqrt{k}} \sum_{i=1}^k D_{\text{KL}}(P_i \| Q_i) \\ &= \frac{1}{\sqrt{k}} \sum_{i=1}^k \sum_{\mathbf{x}} P_i(\mathbf{x}) \log \frac{P_i(\mathbf{x})}{Q_i(\mathbf{x})} \end{aligned} \quad (4)$$

The total loss encourages the cross-attention map to form activation regions that correspond to the specified object count in the input, thereby contributing to the generation of images with accurate object quantities. Finally, the latent \mathbf{z}_t is updated during the denoising process as follows:

$$\mathbf{z}'_t \leftarrow \mathbf{z}_t - \alpha_t \cdot \nabla_{\mathbf{z}_t} \mathcal{L} \quad (5)$$

Here, α_t is a scale factor that controls the magnitude of the gradient step.

Experiments

Experimental setup

We conduct experiments to evaluate how accurately text-to-image generation models reflect the object quantities specified in input prompts. For evaluation, we analyze the generated outputs using two complementary tools: CountGD (Amini-Naieni, Han, and Zisserman 2025), an object counting model built on Grounding DINO (Liu et al. 2025), and the TIFA framework (Hu et al. 2023), which utilizes GPT-4o mini (OpenAI et al. 2024) as its Visual Question Answering (VQA) model. These tools automatically estimate the

Method	Acc.(%) (↑)	MAE. (↓)	RMSE (↓)
SD2.1	23.45	2.235	3.898
Counting Guidance	23.57	2.256	4.522
Ours (SD2.1)	41.87	1.228	2.067
SDXL	27.25	4.350	9.656
Zafar et al.	26.90	1.722	2.675
CountGen	44.80	1.530	3.293
Ours (SDXL)	63.27	0.820	4.670

Table 1: Comparison of object count accuracy in image generation between CountCluster (Ours) and existing methods. The number of objects in the generated images was measured using a counting model, and the results were evaluated with Accuracy, MAE, and RMSE metrics.

number of object instances in each image, and the resulting counts are compared to the quantities specified in the prompts. In these experiments, the proposed method is applied to both SD2.1 and SDXL, with a clustering threshold of $\tau = 0.3$. Further implementation details are provided in the supplementary material.

Benchmark datasets. To quantitatively evaluate the models’ ability to reflect object quantities, we construct a benchmark by integrating prompt sets from prior object counting studies (Binyamin et al. 2024; Kang et al. 2025). Each prompt follows the format “*a photo of [count] [object]*”, where *[count]* is a number word ranging from “*two*” to “*ten*”. This setup enables systematic evaluation across diverse object categories and quantity levels.

Although the benchmark is constructed using relatively simple, quantity-focused prompts, the proposed method is not limited to this set. As discussed in our analysis, it can be effectively extended to complex prompts involving arbitrary quantities, diverse object types, and additional attributes.

Baseline methods. We compare our proposed method with the following five baseline approaches, including those specifically designed to reflect object quantity control. Each baseline is implemented using either SD2.1 or SDXL, and the results are grouped accordingly based on the underlying model architecture.

SD2.1 (Rombach et al. 2022) and SDXL (Podell et al. 2024) are pretrained diffusion models that generate images from prompts without explicit quantity control. Counting Guidance (Kang et al. 2025) estimates object counts at each timestep using RCC (Hobley and Prisacariu 2022) and updates the latent representation based on count discrepancies to guide image generation. CountGen (Binyamin et al. 2024) estimates object counts during generation and regenerates the image if the estimated count does not match the quantity specified in the prompt. To achieve this, it uses the proposed ReLayout model to generate a count-adjusted mask, which is then used to guide the regeneration. Zafar et al. (Zafar, Wolf, and Schwartz 2024) estimate the object instances in the generated image using CLIP-Count (Jiang, Liu, and Chen 2023), learn a count token to reflect the quantity specified in the prompt, and utilize this token at inference time.

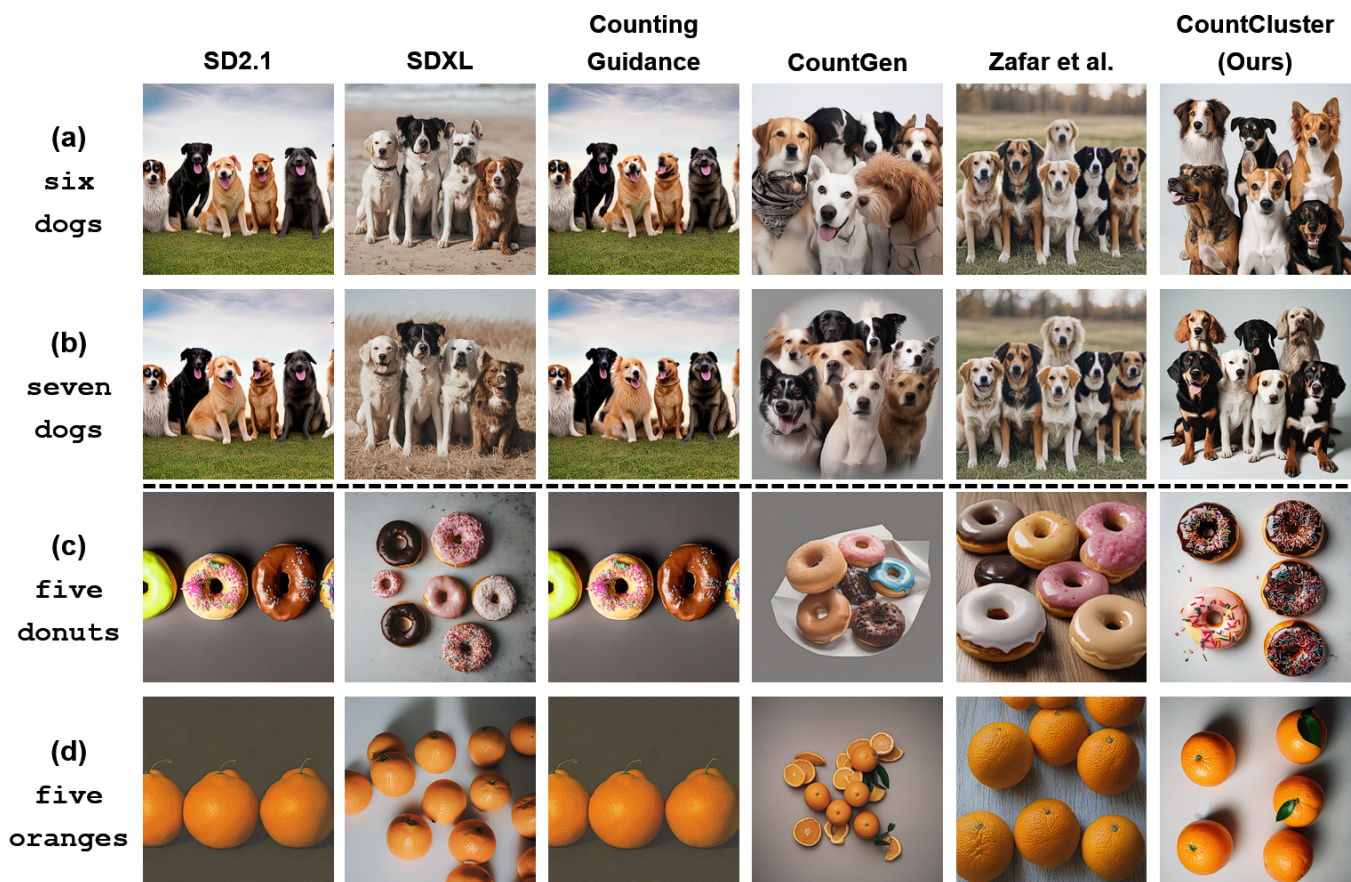


Figure 2: Qualitative results of CountCluster on SDXL and other baseline methods. (a) and (b) show the results of changing only the object quantity in the text prompt (“six” → “seven”) with the same latent. (c) and (d) show the results of changing only the target object (“donuts” → “oranges”) under the same latent.

Qualitative Results

Figure 2 presents a qualitative comparison of images generated by the proposed method and baselines, illustrating the visual effectiveness of each method in reflecting object quantities.

To evaluate the impact of object instance variation on image generation, we generated images from prompts differing only in object count, as illustrated in fig. 2 (a) and (b), while keeping the initial latent fixed. In this experiment, CountCluster accurately captured the increase in the number of dogs corresponding to the prompt, producing consistent results without significantly altering the overall composition or style of the images. In contrast, existing methods exhibited minimal or no change in the generated images despite the increased dog count, often resulting in a mismatch between the number of objects in the images and the quantity described in the prompt. This indicates that baseline models incorporate cross-attention for tokens encoding quantity information relatively weakly, whereas CountCluster is explicitly designed to respond more sensitively to such information.

Additionally, to assess the consistency of quantity control across different object categories, we generated images from

prompts specifying the same object count but varying object types, as shown in fig. 2 (c) and (d), while keeping the initial latent fixed. CountCluster consistently preserve accurate object instances regardless of the object category, whereas existing methods exhibited substantial variability in quantity accuracy depending on the object type. This suggests that prior works rely more heavily on the pretrained priors of the diffusion model of the diffusion model rather than explicit quantity control. In contrast, CountCluster directly manipulates the cross-attention maps to reflect the quantity specified in the prompt, independent of the object category.

Quantitative Results

Object count accuracy and errors. Table 1 presents a quantitative comparison between CountCluster and existing methods on a benchmark dataset. Our SDXL-based method (Ours (SDXL)) achieved the highest Accuracy and lowest MAE, outperforming the original SDXL by 36%p over original SDXL and 18.5%p over CountGen. These results demonstrate CountCluster effectively control object counts through clear separation in cross-attention maps. While RMSE was higher than some baselines because of a few outlier cases where the counting model overestimated object

Method	Counting (%)	Appearing (%)
SD2.1	71.39	99.19
Counting Guidance	71.73	98.89
Ours (SD2.1)	77.95	99.56
SDXL	72.47	99.78
Zafar et al.	74.94	99.11
CountGen	77.01	98.08
Ours (SDXL)	83.16	98.67

Table 2: VQA evaluation results using the TIFA framework. The evaluation was conducted by categorizing questions into Counting and Appearing types.

Method	Time (s)	Mem. (GB)	Training	External
SD2.1	5.89	7	✗	✗
Counting Guidance	21.27	14	✗	✓
Ours (SD2.1)	7.03	8	✗	✗
SDXL	13.32	15	✗	✗
Zafar et al.	9.07	16 (26*)	✓	✗
CountGen	88.04	71	✗	✓
Ours (SDXL)	30.96	20	✗	✗

Table 3: Inference time and memory requirements for each method, along with whether additional training or external modules are used. * indicates requirements during the additional training process.

numbers, the overall metrics confirm our method’s accuracy in reflecting specified quantities.

Ours (SD2.1) also demonstrated an 18.4%p improvement in accuracy compared to the original SD2.1. In addition, it achieved the lowest MAE and RMSE among all SD2.1-based methods, further validating the generality and scalability of the proposed approach across different model architectures.

VQA-guided evaluation of object quantity. Table 2 presents the evaluation results on object count and presence in the generated images using the TIFA framework, which incorporates a GPT-4o mini as VQA model. TIFA conducts two types of questions for each image, object count and object presence, and calculates the accuracy as the Counting score and Appearing score respectively.

The TIFA evaluation results indicate that CountCluster achieves over 6%p improvement in Counting score compared to existing methods, confirming its effectiveness to semantically reflect quantity information. However, the Appearing score was relatively lower, which can be attributed to instances where certain objects were generated with details that differ from those specified in the prompts. For example, cases were observed where a “clock” was classified as an “alarm” or “watch”. These findings suggest that while CountCluster excels at quantity control, it may be disadvantaged in evaluations that require strict semantic consistency.

Inference efficiency and additional resource requirements. Table 3 presents a comparison of inference time, memory consumption, additional training requirements, and

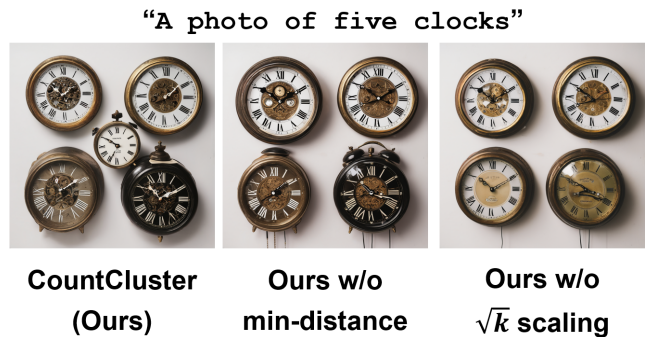


Figure 3: Images generated with the prompt “A photo of five clocks”. (Left) CountCluster. (Middle) Without the minimum distance constraint between cluster centers. (Right) With loss scaling applied using k instead of \sqrt{k} .

Method	Acc.(%) (↑)	MAE. (↓)	RMSE (↓)
Ours (SDXL)	63.27	0.820	4.670
w/o min-distance	47.13	1.430	9.067
w/o \sqrt{k} scaling	44.33	1.249	3.212

Table 4: Ablation study on key components of CountCluster.

inference-time external module dependencies across various methods. All measurements were conducted on a benchmark using four NVIDIA RTX 3090 GPUs.

CountCluster requires longer image generation times compared to SD2.1 and SDXL, as it updates the latent representation via gradient descent. This overhead is particularly pronounced in SDXL due to the increased number of cross-attention layers, leading to substantially higher computational and memory demands and noticeable reductions in speed. In contrast, CountGen exhibited approximately 2.8× times slower inference speeds than CountCluster due to image regeneration, while Counting Guidance was about 3× slower due to the repeated use of external modules. The extended inference time of CountGen is attributed to bottlenecks arising from parallel deployment across four GPUs, indicating that CountGen is designed with high-performance single-GPU or optimized distributed environments in mind.

Additionally, the method proposed by Zafar et al. achieves faster generation speeds by omitting Classifier-Free Guidance (Ho and Salimans 2022); however, it requires training of a count token, which entails approximately 214 seconds of training time and 26 GB of memory, thereby limiting its practical applicability.

Ablation Studies

To thoroughly analyze the effectiveness of the proposed method, ablation studies were conducted to examine the impact of the minimum distance constraint between cluster centers and the KL loss scaling method based on the number of clusters. The evaluation utilized counting model measurements, consistent with previous experiments.

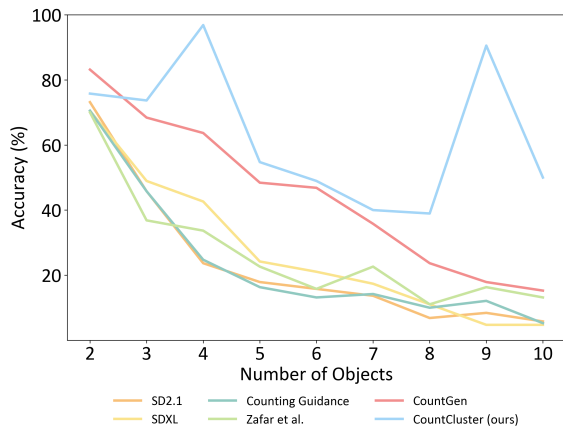


Figure 4: Comparison of quantity accuracy in generated images according to changes in object count.

Effect of minimum distance constraint between cluster centers. The proposed method imposes a minimum distance constraint d between cluster centers to prevent the generation of a single object spanning multiple clusters. Validation results demonstrate that when this minimum distance constraint is applied, images are generated with an accurate number of objects corresponding to the prompt, as illustrated in fig. 3. This is because each cluster corresponds to an independent object.

In contrast, without the minimum distance constraint, a single object may span multiple clusters, resulting in fewer objects than the actual number of clusters and reduced object count accuracy. As shown in table 4, this leads to a 16% decrease in accuracy.

Effect of \sqrt{k} -based loss scaling. CountCluster normalizes the sum of KL divergence losses over k clusters by dividing it by \sqrt{k} . This normalization compensates for the tendency that, as the object count k increases, each cluster occupies a smaller spatial region, causing the total KL loss to increase while the loss per cluster decreases.

When the total KL loss is normalized by dividing by k the loss decreases excessively as the number of clusters increases, leading to under-optimization of the latent representation and resulting in fewer generated objects than specified in the input, as illustrated in fig. 3. Additionally, table 4 shows a 19 percentage point decrease in quantity reflection accuracy compared to when \sqrt{k} scaling is applied. This demonstrates that \sqrt{k} scaling appropriately balances the KL loss, contributing to more stable and accurate reflection of object quantities.

Analysis

Quantitative accuracy analysis across object counts.

Figure 4 presents a comparison of quantity accuracy across methods based on the specified object counts in the benchmark dataset. CountCluster exhibited slightly lower accuracy than CountGen when the object count was two, but achieved higher accuracy than all existing methods for



Figure 5: Images generated by CountCluster from complex prompts.

counts of three or more. Notably, accuracy was particularly high for object counts of four and nine, which can be attributed to the ease of separating activation regions when generating images at square resolutions (512×512 , 1024×1024) arranged in 2×2 and 3×3 grids, respectively.

Existing methods also showed relatively high accuracy at an object count of nine, suggesting that pretrained diffusion models may be more familiar with spatial patterns such as 3×3 grids.

Qualitative evaluation on complex prompts. To evaluate the effectiveness of CountCluster on complex prompts, we conducted additional qualitative analysis. Figure 5 visually presents the results of CountCluster’s quantity control across such complex prompts.

Generated images demonstrate that the cross-attention map can be reliably controlled to maintain accurate object counts, regardless of variations in prompt composition or object attributes. This suggests that CountCluster is capable of robust quantity control that generalizes well across diverse prompts.

Conclusion

In this paper, we introduced CountCluster, a training-free method that enables precise control over object quantities in diffusion-based text-to-image generation. Since the number of objects in the generated image is mostly determined during the early timesteps of the denoising process, our proposed method guides the object cross-attention map to form clearly separated clusters matching the specified object count. Without requiring any external modules or additional training, our method achieved substantial improvements in object count accuracy while maintaining low inference cost. These results highlight the effectiveness and practicality of attention-level intervention for quantity control in generative models.

References

- Agarwal, A.; Karanam, S.; Joseph, K. J.; Saxena, A.; Goswami, K.; and Srinivasan, B. V. 2023. A-STAR: Test-time Attention Segregation and Retention for Text-to-image Synthesis. In *Proceedings of the IEEE/CVF International Conference on Computer Vision (ICCV)*, 2283–2293.
- Amini-Naieni, N.; Han, T.; and Zisserman, A. 2025. COUNTGD: multi-modal open-world counting. In *Proceed-*

- ings of the 38th International Conference on Neural Information Processing Systems, NIPS '24. Red Hook, NY, USA: Curran Associates Inc. ISBN 9798331314385.
- Binyamin, L.; Tewel, Y.; Segev, H.; Hirsch, E.; Rassin, R.; and Chechik, G. 2024. Make It Count: Text-to-Image Generation with an Accurate Number of Objects. *arXiv preprint arXiv:2406.10210*.
- Cao, M.; Wang, X.; Qi, Z.; Shan, Y.; Qie, X.; and Zheng, Y. 2023. MasaCtrl: Tuning-Free Mutual Self-Attention Control for Consistent Image Synthesis and Editing. In *Proceedings of the IEEE/CVF International Conference on Computer Vision (ICCV)*, 22560–22570.
- Chefer, H.; Alaluf, Y.; Vinker, Y.; Wolf, L.; and Cohen-Or, D. 2023. Attend-and-Excite: Attention-Based Semantic Guidance for Text-to-Image Diffusion Models. *ACM Trans. Graph.*, 42(4).
- Couairon, G.; Verbeek, J.; Schwenk, H.; and Cord, M. 2023. DiffEdit: Diffusion-based semantic image editing with mask guidance. In *The Eleventh International Conference on Learning Representations*.
- Dhariwal, P.; and Nichol, A. 2021. Diffusion models beat GANs on image synthesis. In *Proceedings of the 35th International Conference on Neural Information Processing Systems, NIPS '21*. Red Hook, NY, USA: Curran Associates Inc. ISBN 9781713845393.
- Goodfellow, I. J.; Pouget-Abadie, J.; Mirza, M.; Xu, B.; Warde-Farley, D.; Ozair, S.; Courville, A.; and Bengio, Y. 2014. Generative Adversarial Nets. In Ghahramani, Z.; Welling, M.; Cortes, C.; Lawrence, N.; and Weinberger, K., eds., *Advances in Neural Information Processing Systems*, volume 27. Curran Associates, Inc.
- Gu, S.; Chen, D.; Bao, J.; Wen, F.; Zhang, B.; Chen, D.; Yuan, L.; and Guo, B. 2022. Vector Quantized Diffusion Model for Text-to-Image Synthesis. In *Proceedings of the IEEE/CVF Conference on Computer Vision and Pattern Recognition (CVPR)*, 10696–10706.
- Guo, X.; Liu, J.; Cui, M.; Li, J.; Yang, H.; and Huang, D. 2024. InitNO: Boosting Text-to-Image Diffusion Models via Initial Noise Optimization. In *Proceedings of the IEEE/CVF Conference on Computer Vision and Pattern Recognition (CVPR)*, 9380–9389.
- Hertz, A.; Mokady, R.; Tenenbaum, J.; Aberman, K.; Pritch, Y.; and Cohen-or, D. 2023. Prompt-to-Prompt Image Editing with Cross-Attention Control. In *The Eleventh International Conference on Learning Representations*.
- Ho, J.; Jain, A.; and Abbeel, P. 2020. Denoising Diffusion Probabilistic Models. In Larochelle, H.; Ranzato, M.; Hassell, R.; Balcan, M.; and Lin, H., eds., *Advances in Neural Information Processing Systems*, volume 33, 6840–6851. Curran Associates, Inc.
- Ho, J.; and Salimans, T. 2022. Classifier-Free Diffusion Guidance. *arXiv:2207.12598*.
- Hobley, M.; and Prisacariu, V. 2022. Learning to Count Anything: Reference-less Class-agnostic Counting with Weak Supervision. *arXiv:2205.10203*.
- Hu, Y.; Liu, B.; Kasai, J.; Wang, Y.; Ostendorf, M.; Krishna, R.; and Smith, N. A. 2023. TIFA: Accurate and Interpretable Text-to-Image Faithfulness Evaluation with Question Answering. In *Proceedings of the IEEE/CVF International Conference on Computer Vision (ICCV)*, 20406–20417.
- Jiang, R.; Liu, L.; and Chen, C. 2023. CLIP-Count: Towards Text-Guided Zero-Shot Object Counting. In *Proceedings of the 31st ACM International Conference on Multimedia, MM '23*, 4535–4545. New York, NY, USA: Association for Computing Machinery. ISBN 9798400701085.
- Kang, W.; Galim, K.; Koo, H. I.; and Cho, N. I. 2025. Counting guidance for high fidelity text-to-image synthesis. In *2025 IEEE/CVF Winter Conference on Applications of Computer Vision (WACV)*, 899–908. IEEE.
- Karras, T.; Laine, S.; and Aila, T. 2019. A Style-Based Generator Architecture for Generative Adversarial Networks. In *Proceedings of the IEEE/CVF Conference on Computer Vision and Pattern Recognition (CVPR)*.
- Kawar, B.; Zada, S.; Lang, O.; Tov, O.; Chang, H.; Dekel, T.; Mosseri, I.; and Irani, M. 2023. Imagic: Text-Based Real Image Editing with Diffusion Models. In *Conference on Computer Vision and Pattern Recognition 2023*.
- Kullback, S.; and Leibler, R. A. 1951. On information and sufficiency. *The Annals of Mathematical Statistics*, 22(1): 79–86.
- Liu, S.; Zeng, Z.; Ren, T.; Li, F.; Zhang, H.; Yang, J.; Jiang, Q.; Li, C.; Yang, J.; Su, H.; Zhu, J.; and Zhang, L. 2025. Grounding DINO: Marrying DINO with Grounded Pre-training for Open-Set Object Detection. In Leonardis, A.; Ricci, E.; Roth, S.; Russakovsky, O.; Sattler, T.; and Varol, G., eds., *Computer Vision – ECCV 2024*, 38–55. Cham: Springer Nature Switzerland. ISBN 978-3-031-72970-6.
- Lugmayr, A.; Danelljan, M.; Romero, A.; Yu, F.; Timofte, R.; and Van Gool, L. 2022. RePaint: Inpainting Using Denoising Diffusion Probabilistic Models. In *Proceedings of the IEEE/CVF Conference on Computer Vision and Pattern Recognition (CVPR)*, 11461–11471.
- Meng, C.; He, Y.; Song, Y.; Song, J.; Wu, J.; Zhu, J.-Y.; and Ermon, S. 2022. SDEdit: Guided Image Synthesis and Editing with Stochastic Differential Equations. In *International Conference on Learning Representations*.
- Meral, T. H. S.; Simsar, E.; Tombari, F.; and Yanardag, P. 2024. CONFORM: Contrast is All You Need for High-Fidelity Text-to-Image Diffusion Models. In *Proceedings of the IEEE/CVF Conference on Computer Vision and Pattern Recognition (CVPR)*, 9005–9014.
- Nichol, A. Q.; Dhariwal, P.; Ramesh, A.; Shyam, P.; Mishkin, P.; McGrew, B.; Sutskever, I.; and Chen, M. 2022. GLIDE: Towards Photorealistic Image Generation and Editing with Text-Guided Diffusion Models. In Chaudhuri, K.; Jegelka, S.; Song, L.; Szepesvari, C.; Niu, G.; and Sabato, S., eds., *Proceedings of the 39th International Conference on Machine Learning*, volume 162 of *Proceedings of Machine Learning Research*, 16784–16804. PMLR.
- OpenAI; ; Hurst, A.; Lerer, A.; Goucher, A. P.; Perelman, A.; Ramesh, A.; Clark, A.; Ostrow, A.; Welihinda, A.; Hayes, A.; Radford, A.; Madry, A.; Baker-Whitcomb, A.;

Beutel, A.; Borzunov, A.; Carney, A.; Chow, A.; Kirillov, A.; Nichol, A.; Paino, A.; Renzin, A.; Passos, A. T.; Kirillov, A.; Christakis, A.; Conneau, A.; Kamali, A.; Jabri, A.; Moyer, A.; Tam, A.; Crookes, A.; Tootoochian, A.; Tootoochian, A.; Kumar, A.; Vallone, A.; Karpathy, A.; Braunstein, A.; Cann, A.; Codispoti, A.; Galu, A.; Kondrich, A.; Tulloch, A.; Mishchenko, A.; Baek, A.; Jiang, A.; Pelisse, A.; Woodford, A.; Gosalia, A.; Dhar, A.; Pantuliano, A.; Nayak, A.; Oliver, A.; Zoph, B.; Ghorbani, B.; Leimberger, B.; Rossen, B.; Sokolowsky, B.; Wang, B.; Zweig, B.; Hoover, B.; Samic, B.; McGrew, B.; Spero, B.; Giertler, B.; Cheng, B.; Lightcap, B.; Walkin, B.; Quinn, B.; Guaraci, B.; Hsu, B.; Kellogg, B.; Eastman, B.; Lugaresi, C.; Wainwright, C.; Bassin, C.; Hudson, C.; Chu, C.; Nelson, C.; Li, C.; Shern, C. J.; Conger, C.; Barette, C.; Voss, C.; Ding, C.; Lu, C.; Zhang, C.; Beaumont, C.; Hallacy, C.; Koch, C.; Gibson, C.; Kim, C.; Choi, C.; McLeavey, C.; Hesse, C.; Fischer, C.; Winter, C.; Czarnecki, C.; Jarvis, C.; Wei, C.; Koumouzelis, C.; Sherburn, D.; Kappler, D.; Levin, D.; Levy, D.; Carr, D.; Farhi, D.; Mely, D.; Robinson, D.; Sasaki, D.; Jin, D.; Valladares, D.; Tsipras, D.; Li, D.; Nguyen, D. P.; Findlay, D.; Oiwoh, E.; Wong, E.; Asdar, E.; Proehl, E.; Yang, E.; Antonow, E.; Kramer, E.; Peterson, E.; Sigler, E.; Wallace, E.; Brevdo, E.; Mays, E.; Khorasani, F.; Such, F. P.; Raso, F.; Zhang, F.; von Lohmann, F.; Sulit, F.; Goh, G.; Oden, G.; Salmon, G.; Starace, G.; Brockman, G.; Salman, H.; Bao, H.; Hu, H.; Wong, H.; Wang, H.; Schmidt, H.; Whitney, H.; Jun, H.; Kirchner, H.; de Oliveira Pinto, H. P.; Ren, H.; Chang, H.; Chung, H. W.; Kivlichan, I.; O’Connell, I.; O’Connell, I.; Osband, I.; Silber, I.; Sohl, I.; Okuyucu, I.; Lan, I.; Kostrikov, I.; Sutskever, I.; Kanitscheider, I.; Gulrajani, I.; Coxon, J.; Menick, J.; Pachocki, J.; Aung, J.; Betker, J.; Crooks, J.; Lennon, J.; Kiros, J.; Leike, J.; Park, J.; Kwon, J.; Phang, J.; Teplitz, J.; Wei, J.; Wolfe, J.; Chen, J.; Harris, J.; Varavva, J.; Lee, J. G.; Shieh, J.; Lin, J.; Yu, J.; Weng, J.; Tang, J.; Yu, J.; Jang, J.; Candela, J. Q.; Beutler, J.; Landers, J.; Parish, J.; Heidecke, J.; Schulman, J.; Lachman, J.; McKay, J.; Uesato, J.; Ward, J.; Kim, J. W.; Huizinga, J.; Sitkin, J.; Kraaijeveld, J.; Gross, J.; Kaplan, J.; Snyder, J.; Achiam, J.; Jiao, J.; Lee, J.; Zhuang, J.; Harriman, J.; Fricke, K.; Hayashi, K.; Singhal, K.; Shi, K.; Karthik, K.; Wood, K.; Rimbach, K.; Hsu, K.; Nguyen, K.; Gu-Lemberg, K.; Button, K.; Liu, K.; Howe, K.; Muthukumar, K.; Luther, K.; Ahmad, L.; Kai, L.; Itow, L.; Workman, L.; Pathak, L.; Chen, L.; Jing, L.; Guy, L.; Fedus, L.; Zhou, L.; Mamitsuka, L.; Weng, L.; McCallum, L.; Held, L.; Ouyang, L.; Feuvrier, L.; Zhang, L.; Kondraciuk, L.; Kaiser, L.; Hewitt, L.; Metz, L.; Doshi, L.; Afak, M.; Simens, M.; Boyd, M.; Thompson, M.; Dukhan, M.; Chen, M.; Gray, M.; Hudnall, M.; Zhang, M.; Aljube, M.; Litwin, M.; Zeng, M.; Johnson, M.; Shetty, M.; Gupta, M.; Shah, M.; Yatbaz, M.; Yang, M. J.; Zhong, M.; Glaese, M.; Chen, M.; Janner, M.; Lampe, M.; Petrov, M.; Wu, M.; Wang, M.; Fradin, M.; Pokrass, M.; Castro, M.; de Castro, M. O. T.; Pavlov, M.; Brundage, M.; Wang, M.; Khan, M.; Murati, M.; Bavarian, M.; Lin, M.; Yesildal, M.; Soto, N.; Gimelshein, N.; Cone, N.; Staudacher, N.; Summers, N.; LaFontaine, N.; Chowdhury, N.; Ryder, N.; Stathas, N.; Turley, N.; Tezak, N.; Felix, N.; Kudige, N.; Keskar, N.; Deutsch, N.; Bundick, N.; Puckett, N.; Nachum, O.; Okelola, O.; Boiko, O.; Murk, O.; Jaffe, O.; Watkins, O.; Godement, O.; Campbell-Moore, O.; Chao, P.; McMillan, P.; Belov, P.; Su, P.; Bak, P.; Bakkum, P.; Deng, P.; Dolan, P.; Hoeschele, P.; Welinder, P.; Tillet, P.; Pronin, P.; Tillet, P.; Dhariwal, P.; Yuan, Q.; Dias, R.; Lim, R.; Arora, R.; Troll, R.; Lin, R.; Lopes, R. G.; Puri, R.; Miyara, R.; Leike, R.; Gaubert, R.; Zamani, R.; Wang, R.; Donnelly, R.; Honsby, R.; Smith, R.; Sahai, R.; Ramchandani, R.; Huet, R.; Carmichael, R.; Zellers, R.; Chen, R.; Chen, R.; Nigmatullin, R.; Cheu, R.; Jain, S.; Altman, S.; Schoenholz, S.; Toizer, S.; Miserendino, S.; Agarwal, S.; Culver, S.; Ethersmith, S.; Gray, S.; Grove, S.; Metzger, S.; Hermani, S.; Jain, S.; Zhao, S.; Wu, S.; Jomoto, S.; Wu, S.; Shuaiqi, Xia; Phene, S.; Papay, S.; Narayanan, S.; Coffey, S.; Lee, S.; Hall, S.; Balaji, S.; Broda, T.; Stramer, T.; Xu, T.; Gogineni, T.; Christianson, T.; Sanders, T.; Patwardhan, T.; Cunningham, T.; Degry, T.; Dimson, T.; Raoux, T.; Shadwell, T.; Zheng, T.; Underwood, T.; Markov, T.; Sherbakov, T.; Rubin, T.; Stasi, T.; Kaftan, T.; Heywood, T.; Peterson, T.; Walters, T.; Eloundou, T.; Qi, V.; Moeller, V.; Monaco, V.; Kuo, V.; Fomenko, V.; Chang, W.; Zheng, W.; Zhou, W.; Manassra, W.; Sheu, W.; Zaremba, W.; Patil, Y.; Qian, Y.; Kim, Y.; Cheng, Y.; Zhang, Y.; He, Y.; Zhang, Y.; Jin, Y.; Dai, Y.; and Malkov, Y. 2024. GPT-4o System Card. arXiv:2410.21276.

Paiss, R.; Ephrat, A.; Tov, O.; Zada, S.; Mosseri, I.; Irani, M.; and Dekel, T. 2023. Teaching CLIP to Count to Ten. In *Proceedings of the IEEE/CVF International Conference on Computer Vision (ICCV)*, 3170–3180.

Podell, D.; English, Z.; Lacey, K.; Blattmann, A.; Dockhorn, T.; Müller, J.; Penna, J.; and Rombach, R. 2024. SDXL: Improving Latent Diffusion Models for High-Resolution Image Synthesis. In *The Twelfth International Conference on Learning Representations*.

Radford, A.; Kim, J. W.; Hallacy, C.; Ramesh, A.; Goh, G.; Agarwal, S.; Sastry, G.; Askell, A.; Mishkin, P.; Clark, J.; Krueger, G.; and Sutskever, I. 2021. Learning Transferable Visual Models From Natural Language Supervision. In Meila, M.; and Zhang, T., eds., *Proceedings of the 38th International Conference on Machine Learning*, volume 139 of *Proceedings of Machine Learning Research*, 8748–8763. PMLR.

Radford, A.; Metz, L.; and Chintala, S. 2016. Unsupervised Representation Learning with Deep Convolutional Generative Adversarial Networks. arXiv:1511.06434.

Ramesh, A.; Pavlov, M.; Goh, G.; Gray, S.; Voss, C.; Radford, A.; Chen, M.; and Sutskever, I. 2021. Zero-Shot Text-to-Image Generation. In Meila, M.; and Zhang, T., eds., *Proceedings of the 38th International Conference on Machine Learning*, volume 139 of *Proceedings of Machine Learning Research*, 8821–8831. PMLR.

Rassin, R.; Hirsch, E.; Glickman, D.; Ravfogel, S.; Goldberg, Y.; and Chechik, G. 2023. Linguistic Binding in Diffusion Models: Enhancing Attribute Correspondence through Attention Map Alignment. In Oh, A.; Naumann, T.; Globerson, A.; Saenko, K.; Hardt, M.; and Levine, S., eds., *Advances in Neural Information Processing Systems*, volume 36, 3536–3559. Curran Associates, Inc.

- Rombach, R.; Blattmann, A.; Lorenz, D.; Esser, P.; and Ommer, B. 2022. High-Resolution Image Synthesis With Latent Diffusion Models. In *Proceedings of the IEEE/CVF Conference on Computer Vision and Pattern Recognition (CVPR)*, 10684–10695.
- Saharia, C.; Chan, W.; Saxena, S.; Li, L.; Whang, J.; Denton, E. L.; Ghasemipour, K.; Gontijo Lopes, R.; Karagol Ayan, B.; Salimans, T.; Ho, J.; Fleet, D. J.; and Norouzi, M. 2022. Photorealistic Text-to-Image Diffusion Models with Deep Language Understanding. In Koyejo, S.; Mohamed, S.; Agarwal, A.; Belgrave, D.; Cho, K.; and Oh, A., eds., *Advances in Neural Information Processing Systems*, volume 35, 36479–36494. Curran Associates, Inc.
- Tumanyan, N.; Geyer, M.; Bagon, S.; and Dekel, T. 2023. Plug-and-Play Diffusion Features for Text-Driven Image-to-Image Translation. In *Proceedings of the IEEE/CVF Conference on Computer Vision and Pattern Recognition (CVPR)*, 1921–1930.
- Weimin, Q.; Jieke, W.; and Meng, T. 2025. Self-Cross Diffusion Guidance for Text-to-Image Synthesis of Similar Subjects. In *CVPR*.
- Wen, S.; Fang, G.; Zhang, R.; Gao, P.; Dong, H.; and Metaxas, D. 2023. Improving Compositional Text-to-image Generation with Large Vision-Language Models. arXiv:2310.06311.
- Zafar, O.; Wolf, L.; and Schwartz, I. 2024. Iterative Object Count Optimization for Text-to-image Diffusion Models. arXiv:2408.11721.
- Zhang, R.; Chen, Y.; and Lee, K. 2023. Zero-shot Improvement of Object Counting with CLIP. In *RoFoMo: Robustness of Few-shot and Zero-shot Learning in Large Foundation Models*.

Supplementary Material for
**CountCluster: Training-Free Object Quantity Guidance with
 Cross-Attention Map Clustering for Text-to-Image Generation**

Implementation Details

Detailed Experimental Setup

In this study, we implemented our method and determined all hyperparameters with reference to the diffusion pipeline code of Attend-and-Excite (Chefer et al. 2023). The proposed quantity control method was build on both pretrained SD2.1 (Rombach et al. 2022) and SDXL (Podell et al. 2024) models. The object tokens and their quantities were automatically extracted from the prompt using the `inflect` library.

During image generation, the guidance scale (Ho and Salimans 2022) of the diffusion model was fixed at 7.5. In the proposed method, Gaussian smoothing with a kernel size of 3 and $\sigma = 0.5$ was applied to the object cross-attention map, followed by min-max normalization. For the clustering step, we set the attention score threshold $\tau = 0.3$.

The image latent was updated during the first 10 timesteps ($t \in 50, \dots, 40$) of the denoising process. For ours(SD2.1), the scale factor α was set to 40, while for ours(SDXL), it was set to 75,000. Additionally, at t_{50} , iterative refinement was applied until the loss dropped below 0.2, and at t_{40} , refinement continued until the loss reached 0.15 or lower, in order to further optimize the latent.

For image generation, CountGen (Binyamin et al. 2024) utilized four NVIDIA RTX 3090 GPUs in parallel for inference, whereas all other experiments were conducted on a single RTX 3090 GPU. In addition, count token training for the method of Zafar et al. (Zafar, Wolf, and Schwartz 2024) was performed using two RTX 3090 GPUs.

Detailed Benchmark Description

For our experiments, we constructed a benchmark prompt set by integrating those proposed in Counting Guidance (Kang et al. 2025) and CountGen (Binyamin et al. 2024), using prompts of the form “A photo of [count] [object]”. Here, [count] is an English word from two to ten, and [object] is selected from the 19 predefined categories listed in table 5.

Evaluation Metrics

To evaluate the quantity of objects in the generated images, we employed CountGD (Amini-Naieni, Han, and Zisserman 2025) to automatically measure the number of instances in each image corresponding to the object specified in the prompt. The predicted number of instances obtained from

Count	two, three, four, five, six, seven, eight, nine, ten
Object	apples, bears, birds, cars, cats, clocks, dogs, donuts, eggs, elephants, frogs, horses, lemons, mice, monkeys, onions, oranges, tomatoes, turtles

Table 5: List of counts and objects used in the benchmark set

CountGD were then compared with the target counts provided in the prompts to compute the following evaluation metrics: Accuracy (Acc), Mean Absolute Error (MAE), and Root Mean Square Error (RMSE). The formulas for each metric are as follows:

$$\text{Acc} = \sum_{i=1}^n \frac{\mathbf{1}[y_i = \hat{y}_i]}{n} \quad (6)$$

$$\text{MAE} = \sum_{i=1}^n \frac{|y_i - \hat{y}_i|}{n} \quad (7)$$

$$\text{RMSE} = \sqrt{\sum_{i=1}^n \frac{(y_i - \hat{y}_i)^2}{n}} \quad (8)$$

Here, y_i denotes the target object count specified in the i -th prompt, and \hat{y}_i is the number of corresponding object instances in the i -th generated image as predicted by CountGD. n represents the total number of generated images. In our experiments, we evaluated each method on a total of 1,710 images, generated by applying 10 random seeds (0~9) to all 171 combinations of counts and objects.

Additionally, we adopted the TIFA framework (Hu et al. 2023), which utilizes GPT-4o mini (OpenAI et al. 2024) as the VQA model, to jointly evaluate the Counting score and Appearing score. The TIFA score is computed as the proportion of VQA queries for which GPT-4o mini provides the correct answer based on the generated image:

$$\text{TIFA Score} = \sum_{i=1}^n \frac{\mathbf{1}[A_i = \hat{A}_i]}{n} \quad (9)$$

Here, A_i denotes the ground-truth answer for the i -th question, \hat{A}_i represents the answer generated by GPT-4o mini, and n is the total number of question-answer pairs.

The question-answer pairs actually used in the TIFA framework are exemplified in table 6 and table 7:

Prompt: <i>A photo of two apples</i>
Question: How many apples are in the photo?
Choices: 1, 2, 3, 4
Answer: 2

Table 6: Example of Counting VQA

Prompt: <i>A photo of two apples</i>
Question: What fruit is in the photo?
Choices: apples, oranges, bananas, pears
Answer: apples

Table 7: Example of Appearing VQA

Object Cross-attention Map Comparison

fig. 6 shows the visualization results of the object cross-attention maps during image generation with SDXL and SDXL-based CountCluster using the same initial latent. SDXL generates images from a randomly sampled latent distribution, resulting in insufficient control over object quantity. In contrast, our method performs latent updates for quantity control from the beginning, and we observe that cross-attention map clustering is already applied at t_{50} .

More Qualitative Results

To provide additional qualitative comparisons, we compare CountCluster with pretrained diffusion models SD2.1 (Rombach et al. 2022) and SDXL (Podell et al. 2024), as well as with existing object quantity control methods including Counting-guidance (Kang et al. 2025), CountGen (Binyamin et al. 2024), and the method of Zafar et al. (Zafar, Wolf, and Schwartz 2024).

As shown in fig. 7 and fig. 8, existing methods often produce images in which the number of instances does not match the prompt specification, or the individual objects are not clearly separated. In contrast, CountCluster generates images where the specified number of instances is accurately generated and each instance is clearly distinguishable.

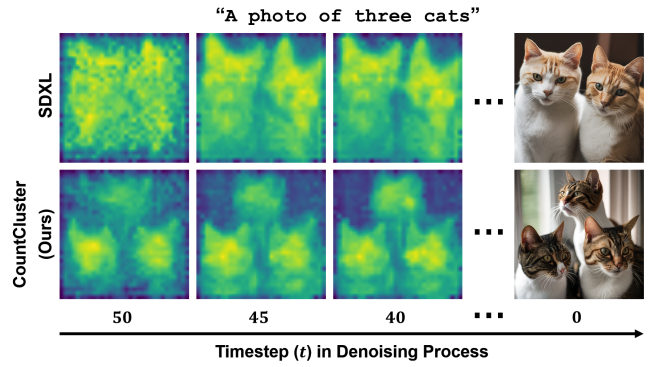


Figure 6: Object cross-attention maps at the early timesteps and generated images from SDXL and CountCluster

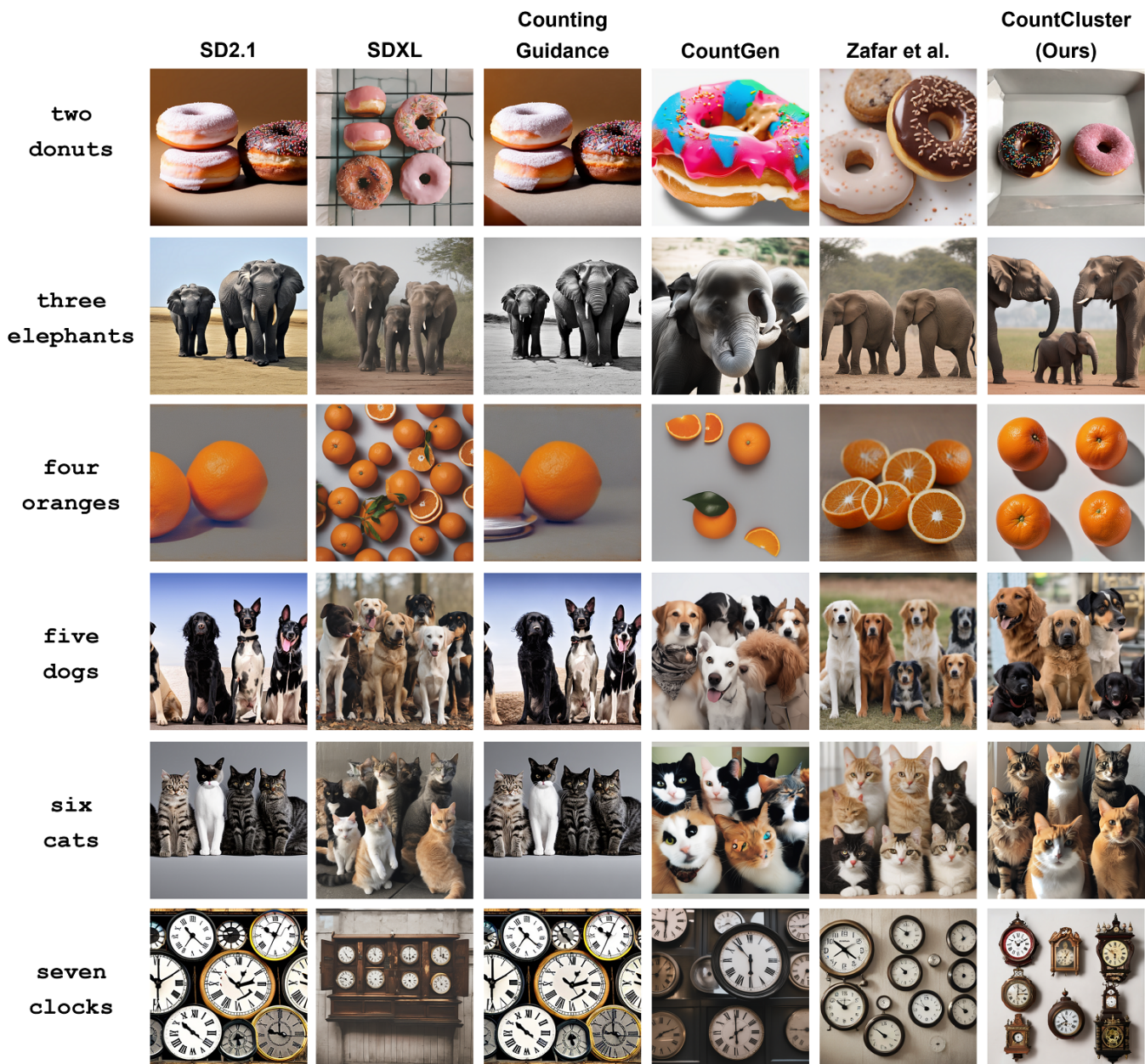


Figure 7: More qualitative comparisons of CountCluster and SD2.1, SDXL, Counting Guidance, CountGen, and Zafar et al.

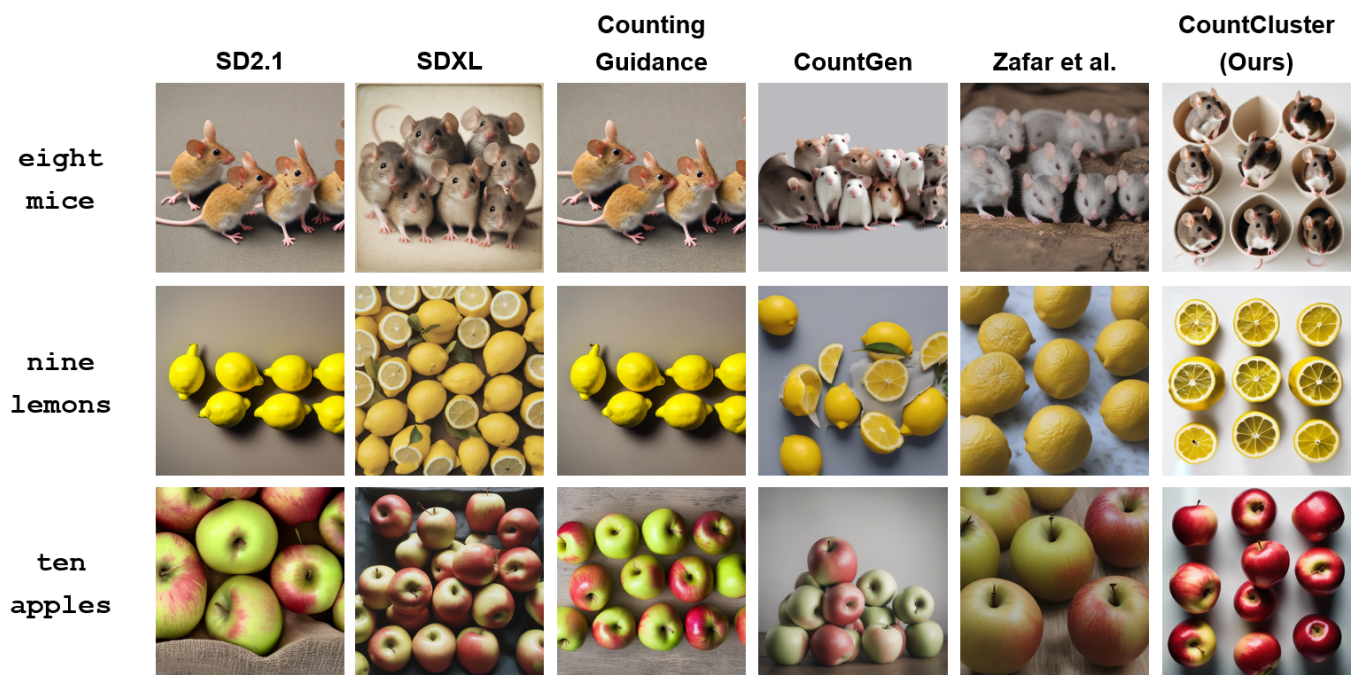


Figure 8: More qualitative comparisons of CountCluster and SD2.1, SDXL, Counting Guidance, CountGen, and Zafar et al.